Multipolar Plasmon Resonances in Individual Ag Nanorice

Hong Wei,[†] Alejandro Reyes-Coronado,[‡] Peter Nordlander,[§] Javier Aizpurua,[‡],* and Hongxing Xu[†,⊥],*

[†]Beijing National Laboratory for Condensed Matter Physics and Institute of Physics, Chinese Academy of Sciences, Box 603-146, Beijing 100190, China, [‡]Centro Mixto de Física de Materiales CSIC-UPV/EHU and Donostia International Physics Center DIPC, San Sebastián 20018, Spain, [§]Department of Physics and Astronomy, Department of Electrical and Computer Engineering, Laboratory for Nanophotonics, Rice University, Houston, Texas 77005, and [⊥]Division of Solid State Physics/The Nanometer Structure Consortium, Lund University, Box 118, S-22100 Lund, Sweden

ABSTRACT We study the optical excitation of high-order surface plasmon resonance modes in individual Ag nanorice particles using dark-field scattering spectroscopy. We analyze the results by model calculations using the boundary element method. Symmetry breaking caused by oblique illumination makes the even order resonance modes observable in the optical spectrum. All the resonance peaks are found to redshift with increasing length of the particle.

KEYWORDS: nanorice · individual nanoparticles · dark-field scattering · multipolar plasmon resonances · oblique excitation

Low-dimensional metallic nanostructures have been the objects of considerable interest during the past decade owing to their support of propagating and localized surface plasmon polaritons (SPPs) and collective oscillations of electron gas at the metal−dielectric interfaces.[1] The localized surface plasmon resonances (LSPRs) in metal nanoparticles (NPs) can result in a drastically enhanced electromagnetic field, which is the physical basis for surface-enhanced Raman scattering (SERS)[2−4] and fluorescence.[5,6] The LSPRs of single NPs depend strongly on their size, shape, material, incident excitation, and environment,[7−9] which facilitates their applications in ultrasensitive sensing,[10,11] surface-enhanced spectroscopy,[12,13] and catalysis.[14]

Among all possible nanoparticle topologies, quasi-one-dimensional nanostructures, that is, nanorods,[6,15−20] nanorice[21] and nanowires,[22,23] have attracted significant interest due to their highly tunable LSPRs and potential to serve as optical waveguides below the diffraction limit. Previous investigations of these structures have mainly focused on the dipolar resonances in small NPs, while multipolar plasmon resonances have only recently begun to attract attention. Multipolar plasmons in nanorod arrays[24] and colloidal ensemble[25] have been investigated by extinction spectroscopy. More recently, the plasmon modes in individual nanorods and nanowires were studied by photoemission electron microscopy (PEEM)[26] and apertureless scanning near field optical microscopy (aSNOM).[18,27] These investigations have shown the existence of high-order localized modes, which are analogous to Fabry−Pérot (FP) modes arising from the reflections between the two ends of the elongated metallic particles.

In this work, we spectroscopically characterize the optical properties of individual Ag nanorice particles. Multipolar longitudinal plasmon resonances in individual rice-shaped nanoparticles are detected by dark-field (DF) scattering spectroscopy. With the increase of particle length, the plasmon resonances redshift and higher order resonance peaks appear. The experimental findings are in excellent agreement with theoretical simulations. To the best of our knowledge, it is the first time that multipolar plasmon resonances of nanorod-like particles are revealed in chemically synthesized individual nanoparticles by means of DF scattering spectroscopy.

RESULTS AND DISCUSSION

Ag nanorice particles were synthesized by the method reported recently.[28] Figure 1a shows a typical scanning electron microscopy (SEM) image of the Ag nanorice particles. The average length is about 320 nm and the width is about 60 nm. The UV−visible−infrared extinction spectrum of nanorice ensemble in ethanol shown in Figure 1b was measured on
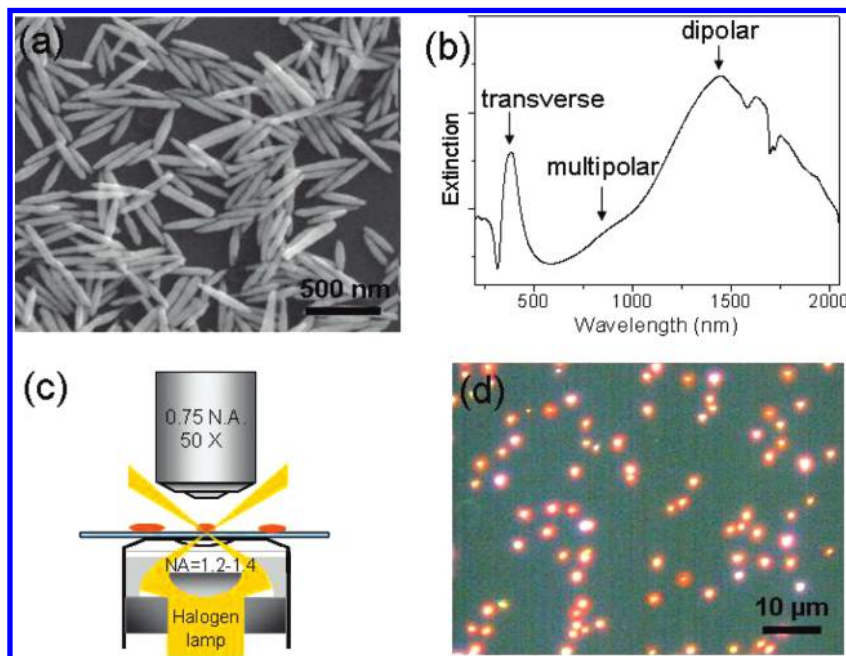
Figure 1. (a) SEM image of Ag nanorice; (b) UV−visible−infrared spectrum of the nanorice ensemble in ethanol; (c) schematic drawing of the dark-field setup; (d) dark-field image of Ag nanorice.

a VARIAN Cary 5000 UV−vis−NIR spectrophotometer. A broad absorption peak in near-infrared at a wavelength of around 1500 nm can be easily identified as
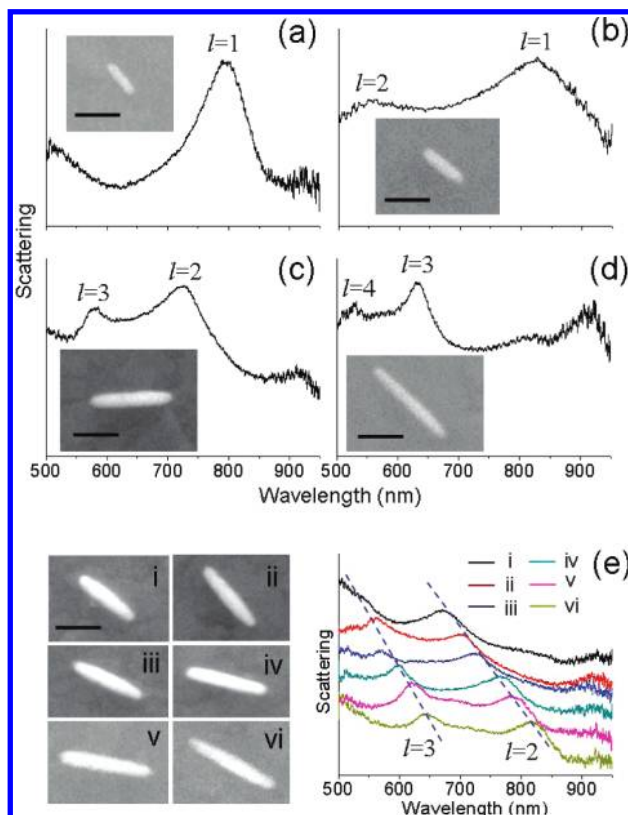

Figure 2. Nonpolarized dark field scattering spectra of Ag nanorice of various lengths: (a) 170, (b) 220, (c) 361, (d) 427, and (e) 300, 328, 335, 363, 417, 436 nm for curves i, ii, iii, iv, v, and vi, respectively. Longitudinal modes of different orders are well-separated and labeled l = 1−4 in panels a−d. Corresponding SEM images are shown in the insets. The scale bar is 200 nm. The dash lines in panel e are eye guides.

the longitudinal dipolar resonance. Both nonhomogenous broadening from size/shape distribution and radiative decay in each particle contribute to the spectral broadening of the resonance. As will be demonstrated below using simulations, the sharp transverse mode at a wavelength of about 385 nm is a superposition of several transverse modes, and the weak shoulder at a wavelength of about 860 nm is a mixture of multipolar plasmon resonances of different orders. This shoulder was reported as well in our previous paper,[28] but the dipolar resonant peak was out of the measurement range of the HITACHI U-3010 UV−vis spectrophotometer used at that time, and the shoulder peak was deformed due to the imperfect response of the instrument close to the limitation of the measurement range. The extinction spectra of nanorice colloids measured with the different instruments are shown in the Supporting Information (Figure S1).

The dark-field experiment setup is based on a Leica DM LM microscope and schematically shown in Figure 1c. Figure 1d shows a typical dark field image for Ag nanorice particles. To study the scattering properties of individual nanorice, a sparser particle density was used.

To theoretically analyze the experimental results, we performed extensive simulations of the optical extinction cross section of an individual particle with the boundary element method (BEM).[29] All the nanorice particles were assumed to be perfect spheroids. The propagating direction and polarization of the incident plane wave were both aligned 45° with respect to the spheroid axis, a configuration that allows the simultaneous excitation of both transverse and longitudinal modes of arbitrary orders.[30] The spheroid widths were

kept constant at 60 nm in all the calculations. The effect of the substrate was taken into account by assuming an effective index of refraction $n_{eff} = 1.2585$ for the medium surrounding the nanoparticle, obtained from a simple average of the air and substrate dielectric constants $\varepsilon_{eff} = (\varepsilon_{air} + \varepsilon_{glass})/2$.

Measured scattering spectra of individual nanorice particles of various dimensions and the corresponding SEM images are shown in Figure 2. For small particle sizes, the longitudinal dipolar resonance ($l = 1$) at $\lambda = 794$ nm is apparent (see Figure 2a). Similar to single particle studies on small gold nanorods,[31,32] this dipolar mode exhibits significant radiative broadening. Owing to the oblique excitation, symmetry-forbidden modes of even parity become optically active, as labeled $l = 2$ and $l = 4$ in Figure 2b−d.[30] With increasing length of the particle, the second order resonance peak grows in amplitude and red-shifts, and the third ($l = 3$) and the fourth ($l = 4$) order longitudinal resonance peaks appear in the spectra (Figure 2c,d). In Figure 2e, DF spectra of six nanorice particles of different lengths are shown, in which the redshift of the $l = 2$ and $l = 3$ resonances can be clearly seen. BEM calculations of the optical extinction in a larger spectral range also show these peak shifts (Supporting Information, Figure S2).

To make the mode assignments more clear, we plot the length of nanorice versus the experimental peak positions of the optical extinction obtained from DF spectroscopy for hundreds of individual nanoparticles, as shown with black points in Figure 3. The experimental dots fall into four distinct bands, divided in the figure by white dashed lines. These bands can be associated to four well-defined orders of plasmon modes, similar to previous ensemble studies of rod-shaped particles.[24,25] A contour plot of the extinction cross-section of 60 nm-wide nanorice particles of various lengths calculated by BEM is presented as the background of Figure 3. Excellent overall agreement with experimental data for the spectral position of the different orders is obtained. Longitudinal resonant peaks of different orders shift to the red with increasing particle length. The shifting rates decrease with the increase of the order of the resonance. For clarity, the simulation data along the horizontal white line in the contour plot is drawn out and plotted as an extinction spectrum corresponding to a nanorice particle of length equal to 400 nm, which is shown at the bottom of Figure 3.

Since the energy of the LSPRs here lies well below the interband threshold of Ag (3.86 eV), the damping of multipolar plasmon resonances in Ag nanorice can be attributed primarily to Drude damping and radiative damping. As shown in Figure 3, for a nanorice particle of a given length, lower order modes always present broader peaks and exhibit larger radiative damping. In this case, the nanorice acts as an effective antenna. On the contrary, as observed in the contour plot of Figure 3, higher order modes can serve as high-quality electro-
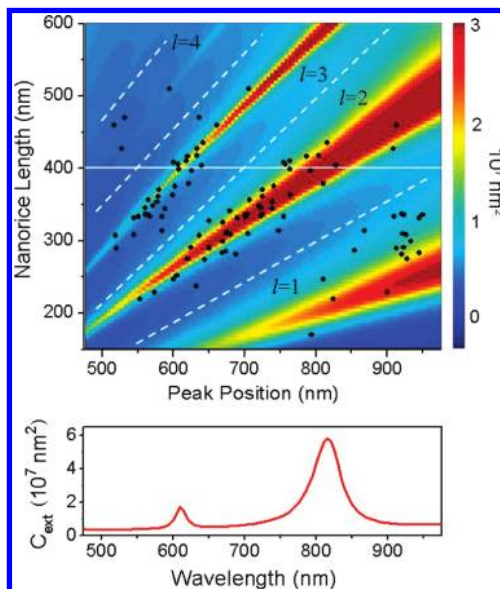

Figure 3. (Top) Dependence of LSPR peak positions on nanorice lengths. Black dots: Dark-field scattering peak positions of different resonance orders for nanorice particles of different lengths determined from experiments. Four distinct bands separated by the dashed white lines are apparent, each of which corresponds to a well-defined mode marked from $l = 1$ to $l = 4$. Background: Extinction cross-section of individual nanorice (rice width equal to 60 nm) calculated from BEM simulations assuming an effective dielectric surrounding, $n_{eff} = 1.2585$. Incident direction and polarization were both aligned 45° with respect to the symmetry axis of the nanorice. The white dashed lines are plotted for eyeguiding. (Bottom) Extinction coefficient extracted from the horizontal white line on the top contour plot for a nanorice with a length of 400 nm. Two modes appear in the spectrum for this length.

magnetic modes thanks to their lower radiative loss. For a given mode order l, the intensity of the peak grows with increasing particle length, and the radiative loss increases as well. Since the emission power is proportional to the square of the polarization momentum, within the description given by a classical harmonic oscillator, stronger oscillator strength is therefore generated in longer particles. Thus, excitation of higher order modes will lead to higher local field confinement, one primary objective in both solar energy harvesting and enhanced spectroscopy, such as SERS and enhanced fluorescence.[33]

For a better understanding of the multiple LSPRs in nanorice, we calculated the electric near-field distributions for a particle of 500 nm length and 60 nm width. The excitation configuration is shown in Figure 4a, where the incident plane wave is at an angle θ with respect to the main axis of the particle, while linear polarization is kept within the incident plane. The extinction cross-section in Figure 4b shows the resonance positions under oblique excitation (θ = 45° is selected as a representation of the oblique incidence). Five distinct longitudinal resonances at wavelengths λ of 1717.5, 972.5, 715, 590, and 519 nm appear in the extinction spectrum, corresponding to the first five multipolar
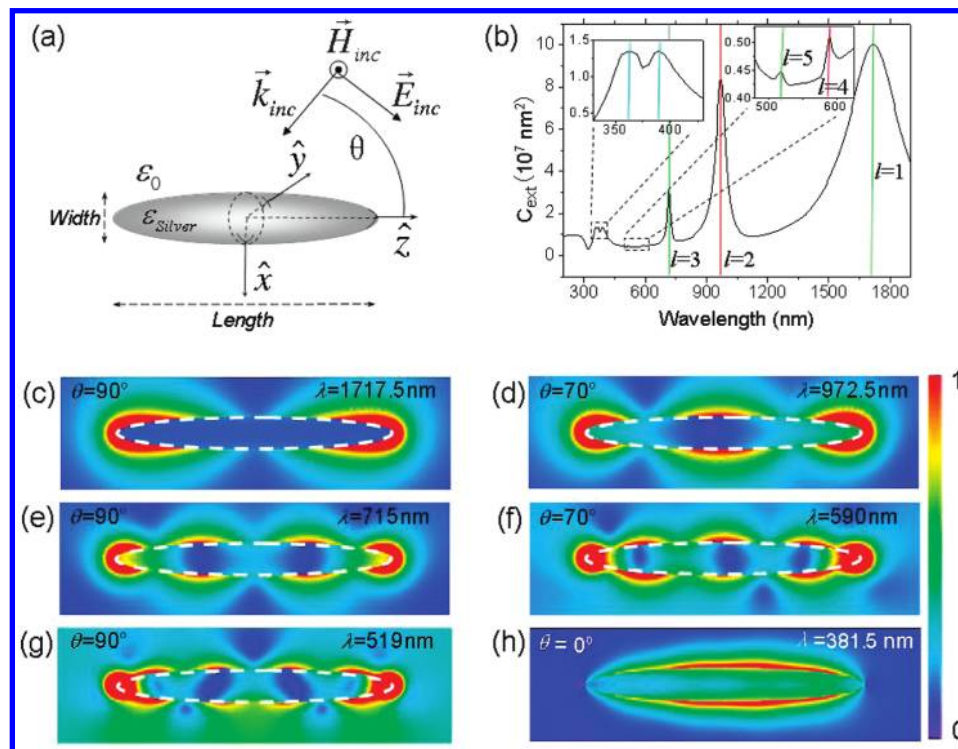
Figure 4. (a) Schematics of the geometry used in the simulations. (b) Simulated extinction cross section for particle of 500 nm length and 60 nm width and an incident angle θ = 45°. The inset to the right-hand side is a zoom of the 4th and 5th longitudinal modes, whereas the inset to the left-hand side is a zoom of the transversal modes. (c−h) Local electric field distribution in the plane x−z induced by oblique incidence excitation at different incident angles θ at the resonant wavelengths λ marked in panel b. The angles of incidence for the near-field distributions are selected to give emphasis to the particular mode under study.

modes. The peaks at λ = 362.5 and λ = 389 nm (cyan lines in the left-hand side inset of Figure 4b) are transverse modes, and do not show significant shifts with particle length. It should be noted that under normal incidence (θ = 90°), with polarization aligned along the nanorice axis, only odd modes (l = 1, 3, 5, indicated by green lines in Figure 4b and the inset) can be excited. Both the longitudinal even modes (l = 2, 4, red lines in Figure 4b and the right-hand side inset) and the transverse modes at λ = 362.5 and λ = 389 nm are absent in the spectrum in the case of normal incidence due to symmetry reasons (Supporting Information, Figure S3a). For oblique excitation, the relative intensity of different peaks depends on the angle of incidence (Supporting Information, Figure S3b). In the zoom plot of the transverse modes (left-hand side inset of Figure 4b), it can be seen that the peak at λ = 362.5 nm is quite broad and looks like a superposition of different modes. To get more insights about these transverse modes, we improved the resolution in the simulations and calculated the activation of transverse modes in different excitation configurations (Supporting Information, Figure S4). The results of these calculations show that the actual position of the first transverse mode peak is at λ = 381.5 nm. The nature of the modes can be identified by analyzing the near-field distribution around the particle. Since the spectral position of the modes does not change significantly (Supporting Information, Figure

S3c,d), we choose different incident angles, which are complementary to the incidence angle shown in Figure 4b, to show the near-field distribution of the modes in Figure 4c−h. The selected incidence angles (displayed on the top left-hand side of each plot) correspond to cases where the particular mode under study is excited very efficiently; that is, situations where the strength of a given mode is large. Quasi-standing-wave patterns are clearly observable in the normalized near field plots of Figure 4c−h. As expected, for normal incidence (θ = 90°) odd-order modes are excited (Figure 4c,e,g). The dipolar mode (l = 1 in Figure 4c) presents a node at the center of the particle, while two, three, four, and five nodes are present for the second (l = 2 in Figure 4d), third (l = 3 in Figure 4e), fourth (l = 4 in Figure 4f), and fifth (l = 5 in Figure 4g) longitudinal modes, respectively. Oblique incidence-induced symmetry breaking ensures the excitation of otherwise forbidden modes, (see Figure 4d,f for an incidence of θ = 70°). The near-field distribution corresponding to the excitation of a transverse mode is also displayed in Figure 4h allowing for immediate identification of its transverse nature. An important observation from the calculated near-field distribution is that electromagnetic energy penetrates drastically into the surrounding medium mainly at the nanoparticle ends enabling possibilities for applications of these particles in sensing.

In summary, we have observed high-order surface plasmon resonance modes in individual Ag nanorice particles. Recently, some interesting applications based on the elongated taper-ended nanostructures have been theoretically proposed, such as single atom trapping[34] and metamaterials for optical cloaking[35] as well as subwavelength color imaging.[36] We suggest that Ag nanorice is a highly suitable substrate for LSPR sensing, due to the high sensitivity of the longitudinal resonances on the surrounding environments (Supporting Information, Figures S5,S6). For a nanorice particle of 400 nm length and 60 nm width, the peak shift for the $l = 1$ longitudinal mode is 1114 nm per refractive index unit, which is more sensitive to the environmental refractive index change than that reported in the literature.[37−39] The multipolar plasmon resonances in the visible to near-infrared range also make nanorice particles suitable as substrates in surface-enhanced spectroscopy applications (Supporting Information, Figure S7).

METHODS

Synthesis of Nanorice Particles. High throughput synthesis of Ag nanorice was recently reported,[28] using poly(vinyl pyrrolidone) (PVP) as surfactant and poly(ethylene glycol) 600 (PEG 600) as reducing agent. In brief, 0.5 mL of 1 M $AgNO_3$ aqueous solution and 2.5 mL of 1 M PVP ($M_w \approx 40\,000$; the concentration was calculated in terms of the repeating unit) aqueous solution were added to 25 mL of PEG 600 in a flask under stirring. The flask was transferred to an oil bath and warmed up at 70 °C for 0.5 h, and then heated at 100 °C for about 8 h. All chemicals were purchased from Beijing Chemical Reagents Company. The synthesized Ag nanorice particles are centrifuged in ethanol three times to remove the adsorbed chemicals and finally dispersed in ethanol.

Measurements of Dark-Field Scattering Spectra. The dark-field experiment setup is based on a Leica DM LM microscope. Nonpolarized white light from a halogen lamp was directed from the bottom into a transmission-type dark-field condenser (Olympus, 1.2−1.4 NA). The light scattered by the sample was collected by a 50× objective (Leica, 0.75 NA) and directed to a confocal Raman spectroscopy system (Renishaw, inVia) equipped with a 1800-line/mm grating with an air-cooled CCD. The nanorice particles in ethanol were dispersed on 3-aminopropyl-trimethoxysilane (APTMS)-coated ITO glass substrate.[40] Then, a commercial copper grid (Ted Pella, Inc., Redding, CA) with clear markers was attached to the sample, guaranteeing the direct correlation of dark-field spectra to the SEM images.

Supporting Information Available: Extinction spectrum of nanorice colloid, extinction spectra for different particle lengths, calculated extinction spectra and local electric field distribution of a nanorice particle excited with different incident angle, transverse resonance modes excited under different incidence configurations, sensitivity of plasmon resonances to the environmental refractive index, and SERS measurements on individual nanorice particles. This material is available free of charge *via* the Internet at http://pubs.acs.org.

REFERENCES AND NOTES

1. Barnes, W. L.; Dereux, A.; Ebbesen, T. W. Surface Plasmon Subwavelength Optics. *Nature* **2003**, *424*, 824–830.
2. Xu, H. X.; Bjerneld, E. J.; Kall, M.; Borjesson, L. Spectroscopy of Single Hemoglobin Molecules by Surface Enhanced Raman Scattering. *Phys. Rev. Lett.* **1999**, *83*, 4357–4360.
3. Xu, H. X.; Aizpurua, J.; Kall, M.; Apell, P. Electromagnetic Contributions to Single-Molecule Sensitivity in Surface-Enhanced Raman Scattering. *Phys. Rev. E* **2000**, *62*, 4318–4324.
4. Wei, H.; Hao, F.; Huang, Y. Z.; Wang, W. Z.; Nordlander, P.; Xu, H. X. Polarization Dependence of Surface-Enhanced Raman Scattering in Gold Nanoparticle−Nanowire Systems. *Nano Lett.* **2008**, *8*, 2497–2502.
5. Tam, F.; Goodrich, G. P.; Johnson, B. R.; Halas, N. J. Plasmonic Enhancement of Molecular Fluorescence. *Nano Lett.* **2007**, *7*, 496–501.
6. Aizpurua, J.; Bryant, G. W.; Richter, L. J.; de Abajo, F. J. G.; Kelley, B. K.; Mallouk, T. Optical Properties of Coupled Metallic Nanorods for Field-Enhanced Spectroscopy. *Phys. Rev. B* **2005**, *71*, 235420.
7. Kelly, K. L.; Coronado, E.; Zhao, L. L.; Schatz, G. C. The Optical Properties of Metal Nanoparticles: The Influence of Size, Shape, And Dielectric Environment. *J. Phys. Chem. B* **2003**, *107*, 668–677.
8. Hutter, E.; Fendler, J. H. Exploitation of Localized Surface Plasmon Resonance. *Adv. Mater.* **2004**, *16*, 1685–1706.
9. Shuford, K. L.; Lee, J.; Odom, T. W.; Schatz, G. C. Optical Properties of Gold Pyramidal Shells. *J. Phys. Chem. C* **2008**, *112*, 6662–6666.
10. Willets, K. A.; Van Duyne, R. P. Localized Surface Plasmon Resonance Spectroscopy and Sensing. *Annu. Rev. Phys. Chem.* **2007**, *58*, 267–297.
11. Stewart, M. E.; Anderton, C. R.; Thompson, L. B.; Maria, J.; Gray, S. K.; Rogers, J. A.; Nuzzo, R. G. Nanostructured Plasmonic Sensors. *Chem. Rev.* **2008**, *108*, 494–521.
12. Kneipp, K.; Moskovits, M.; Kneipp, H. *Surface-Enhanced Raman Scattering: Physics and Applications*; Springer: New York, 2006.
13. Lakowicz, J. R. Radiative Decay Engineering 5: Metal-Enhanced Fluorescence and Plasmon Emission. *Anal. Biochem.* **2005**, *337*, 171–194.
14. Larsson, E. M.; Langhammer, C.; Zoric, I.; Kasemo, B. Nanoplasmonic Probes of Catalytic Reactions. *Science* **2009**, *326*, 1091–1094.
15. Schider, G.; Krenn, J. R.; Hohenau, A.; Ditlbacher, H.; Leitner, A.; Aussenegg, F. R.; Schaich, W. L.; Puscasu, I.; Monacelli, B.; Boreman, G. Plasmon Dispersion Relation of Au and Ag Nanowires. *Phys. Rev. B* **2003**, *68*, 155427.
16. Bryant, G. W.; De Abajo, F. J. G.; Aizpurua, J. Mapping the Plasmon Resonances of Metallic Nanoantennas. *Nano Lett.* **2008**, *8*, 631–636.
17. Cubukcu, E.; Capasso, F. Optical Nanorod Antennas As Dispersive One-Dimensional Fabry−Peacuterot resonators for surface plasmons. *Appl. Phys. Lett.* **2009**, *95*, 201101.
18. Dorfmuller, J.; Vogelgesang, R.; Weitz, R. T.; Rockstuhl, C.; Etrich, C.; Pertsch, T.; Lederer, F.; Kern, K. Fabry−Perot Resonances in One-Dimensional Plasmonic Nanostructures. *Nano Lett.* **2009**, *9*, 2372–2377.
19. Novotny, L. Effective Wavelength Scaling for Optical Antennas. *Phys. Rev. Lett.* **2007**, *98*, 266802.
20. Encina, E. R.; Coronado, E. A. Resonance Conditions for Multipole Plasmon Excitations in Noble Metal Nanorods. *J. Phys. Chem. C* **2007**, *111*, 16796–16801.

21. Wang, H.; Brandl, D. W.; Le, F.; Nordlander, P.; Halas, N. J. Nanorice: A Hybrid Plasmonic Nanostructure. *Nano Lett.* **2006**, *6*, 827–832.

22. Ditlbacher, H.; Hohenau, A.; Wagner, D.; Kreibig, U.; Rogers, M.; Hofer, F.; Aussenegg, F. R.; Krenn, J. R. Silver Nanowires As Surface Plasmon Resonators. *Phys. Rev. Lett.* **2005**, *95*, 257403.

23. Li, Z. P.; Hao, F.; Huang, Y. Z.; Fang, Y. R.; Nordlander, P.; Xu, H. X. Directional Light Emission from Propagating Surface Plasmons of Silver Nanowires. *Nano Lett.* **2009**, *9*, 4383–4386.

24. Krenn, J. R.; Schider, G.; Rechberger, W.; Lamprecht, B.; Leitner, A.; Aussenegg, F. R.; Weeber, J. C. Design of Multipolar Plasmon Excitations in Silver Nanoparticles. *Appl. Phys. Lett.* **2000**, *77*, 3379–3381.

25. Payne, E. K.; Shuford, K. L.; Park, S.; Schatz, G. C.; Mirkin, C. A. Multipole Plasmon Resonances in Gold Nanorods. *J. Phys. Chem. B* **2006**, *110*, 2150–2154.

26. Douillard, L.; Charra, F.; Korczak, Z.; Bachelot, R.; Kostcheev, S.; Lerondel, G.; Adam, P. M.; Royer, P. Short-Range Plasmon Resonators Probed by Photoemission Electron Microscopy. *Nano Lett.* **2008**, *8*, 935–940.

27. Jones, A. C.; Olmon, R. L.; Skrabalak, S. E.; Wiley, B. J.; Xia, Y. N. N.; Raschke, M. B. Mid-IR Plasmonics: Near-Field Imaging of Coherent Plasmon Modes of Silver Nanowires. *Nano Lett.* **2009**, *9*, 2553–2558.

28. Liang, H. Y.; Yang, H. X.; Wang, W. Z.; Li, J. Q.; Xu, H. X. High-Yield Uniform Synthesis and Microstructure-Determination of Rice-Shaped Silver Nanocrystals. *J. Am. Chem. Soc.* **2009**, *131*, 6068–6069.

29. Garcia de Abajo, F. J.; Howie, A. Retarded Field Calculation of Electron Energy Loss in Inhomogeneous Dielectrics. *Phys. Rev. B* **2002**, *65*, 115418.

30. Hao, F.; Larsson, E. M.; Ali, T. A.; Sutherland, D. S.; Nordlander, P. Shedding Light on Dark Plasmons in Gold Nanorings. *Chem. Phys. Lett.* **2008**, *458*, 262–266.

31. Sonnichsen, C.; Franzl, T.; Wilk, T.; von Plessen, G.; Feldmann, J.; Wilson, O.; Mulvaney, P. Drastic Reduction of Plasmon Damping in Gold Nanorods. *Phys. Rev. Lett.* **2002**, *88*, 077402.

32. Muskens, O. L.; Bachelier, G.; Del Fatti, N.; Vallee, F.; Brioude, A.; Jiang, X. C.; Pileni, M. P. Quantitative Absorption Spectroscopy of a Single Gold Nanorod. *J. Phys. Chem. C* **2008**, *112*, 8917–8921.

33. Laurent, G.; Felidj, N.; Aubard, J.; Levi, G.; Krenn, J. R.; Hohenau, A.; Schider, G.; Leitner, A.; Aussenegg, F. R. Evidence of Multipolar Excitations in Surface Enhanced Raman Scattering. *Phys. Rev. B* **2005**, *71*, 045430.

34. Chang, D. E.; Thompson, J. D.; Park, H.; Vuletic, V.; Zibrov, A. S.; Zoller, P.; Lukin, M. D. Trapping and Manipulation of Isolated Atoms Using Nanoscale Plasmonic Structures. *Phys. Rev. Lett.* **2009**, *103*, 123004.

35. Cai, W. S.; Chettiar, U. K.; Kildishev, A. V.; Shalaev, V. M. Optical Cloaking with Metamaterials. *Nat. Photonics* **2007**, *1*, 224–227.

36. Kawata, S.; Ono, A.; Verma, P. Subwavelength Colour Imaging with a Metallic Nanolens. *Nat. Photonics* **2008**, *2*, 438–442.

37. Lyvers, D. P.; Moon, J. M.; Kildishev, A. V.; Shalaev, V. M.; Wei, A. Gold Nanorod Arrays as Plasmonic Cavity Resonators. *ACS Nano* **2008**, *2*, 2569–2576.

38. Lee, K. S.; El-Sayed, M. A. Gold and Silver Nanoparticles in Sensing and Imaging: Sensitivity of Plasmon Response to Size, Shape, And Metal Composition. *J. Phys. Chem. B* **2006**, *110*, 19220–19225.

39. Yu, C. X.; Irudayaraj, J. Multiplex Biosensor Using Gold Nanorods. *Anal. Chem.* **2007**, *79*, 572–579.

40. Xu, H. X.; Kall, M. Polarization-Dependent Surface-Enhanced Raman Spectroscopy of Isolated Silver Nanoaggregates. *Chemphyschem* **2003**, *4*, 1001–1005.